

Article

Novel Design and Implementation of a Knee Exoskeleton for Gait Rehabilitation with Impedance Control Strategy

Nattapat Kieuvongngam^{1,a}, Anan Sutapun^{2,b}, and Viboon Sangeveraphunsiri^{3,c,*}

¹ Department of Mechanical Engineering, Faculty of Engineering, Chulalongkorn University, 254 Phayathai Rd., Pathumwan, Bangkok 10330, Thailand

² Haxter Robotics, Bangkok 10330, Thailand

³ Faculty of Engineering, Chulalongkorn University, Bangkok 10330, Thailand

E-mail: ^anattapatkieu@gmail.com, ^banansutapun@gmail.com,

^{c,*}viboon.s@chula.ac.th (Corresponding author)

Abstract. This paper presents a novel cable-driven robotic joint for a gait exoskeleton robot. We discussed in detail a lightweight, low inertia, and highly back-drivable, 1-DOF tension amplification mechanism based on a pulley system and block-and-tackle technique. The exoskeleton is controlled using an impedance controller under the active-assistive and resistive approaches. Four experiments were conducted to evaluate the proposed exoskeleton's safety and controller performance: mechanical transparency analysis, active-assistive trajectory tracking, resistance of trajectory tracking, and gait rehabilitation. The exoskeleton demonstrated high transparency with the root mean square (RMS) torque of 0.457 Nm under no-load condition, suggesting that the mechanism is highly back-drivable, has a low moment of inertia, and is mechanically safe to operate. The active-assistive trajectory tracking experiment indicated that the output torque was generated under assist-as-needed approach, as the average robotic-assistance torque was lowered by more than 73% when the user provided assistance force to complete the task on their own. Additionally, the resistance experiment revealed the feasibility of employing the exoskeleton to strengthen muscles with adjustable resistive torque from 0.94 Nm and 2.25 Nm. Finally, the result of gait rehabilitation experiment demonstrated that the robot was able to provide adequate torque to assist users in completing their gait cycle without causing any negative effects during or after the experiment.

Keywords: Gait exoskeleton robot, rehabilitation robot, cable-driven mechanism, impedance control, active assistive control strategy.

ENGINEERING JOURNAL Volume 26 Issue 11

Received 22 June 2022

Accepted 21 November 2022

Published 30 November 2022

Online at <https://engj.org/>

DOI:10.4186/ej.2022.26.11.13

1. Introduction

Walking disability is a common occurrence for post-stroke patients, making it more difficult for them to carry out their everyday activities [1]. Stroke not only affects the individual but also the society as a whole. Caretakers and physiotherapists are required to assist and care for patients for the majority of the time as well as the social consequences of stroke in working-aged adults. Along with medical expenses, patients also need intensive rehabilitation to effectively recover from impairment [1-3]. A recent study indicates that the most effective way to enhance stroke recovery is via intense and repetitive functional training and by getting treatment in an early stage [4], [5]. As a consequence, over the last decade, a wide variety of gait rehabilitation robots have been developed to address the issues [6-13]. Using robot-assisted rehabilitation not only reduces therapists' workloads, by allowing a single therapist to supervise multiple rehabilitation sessions simultaneously, but also improves treatment outcomes [3], with over 75% improvement in a variety of metrics such as ambulation, mobility, and balance indicators [2].

Traditional gait rehabilitation robots can be classified into two categories based on their actuated joints and configuration: complete exoskeletons and partial exoskeletons. For complete exoskeletons, the robot shall be actuated in at least four joints: two in the hips and two in the knees. Thus, the complete exoskeletons can provide total support for the users sagittal plane motions and can incorporate additional assistance functions like sit-to-stand transition [14] and climbing and descending stairs [15]. Additionally, the active joints in the complete exoskeleton type may exceed ten DOFs [17], allowing a hands-free operation in both sagittal and lateral planes for more realistic training. Partial exoskeletons, on the other hand, must have at least one motorized joint but not enough to be classified as a complete exoskeleton. The ExLeg lower-limb rehabilitation robot, for instance, is designed in a seated position [12], [16] and has three actuated-joints at the hip, knee, and ankle. However, this type of robot usually operates in a single leg configuration [18], [19], with the actuated joint located only at the knee to allow regular gait training [13]. In comparison to complete exoskeletons, partial exoskeletons are lighter, smaller, and simpler to model and control. However, in terms of functionality, partial exoskeletons offer less stability, impose more restrictions on the patient's requirements, and cannot operate in a hands-free condition [13].

The first consideration in the design of an exoskeleton robot is user safety. ISO10218 suggests that to effectively promote safety, the amount of energy transferred from robot to human during contact should be reduced to a minimum. This may be achieved mechanically by including lightweight, low inertia, and highly back-drivable criteria into the mechanical design [20], [21]. In terms of controller design, the control algorithm shall be capable of ensuring high stability and generating an appropriate

amount of output torque. And the robot should operate within a suitable range of velocity. This can be accomplished by utilizing the force-position control approach where the force control is in the inner-loop and the outer-loop is a position control.



Fig. 1. The proposed knee exoskeleton with mechanical components and its range of motion during the walking stage.

Typical exoskeletons consist of an actuator, a gearbox or a power transmission system, and a soft brace or a flexible frame to help for the user attachment. Numerous concepts have been investigated and put into practice. Series elastic actuators (SEAs) are one of the most prevalent actuators and transmission systems used in exoskeletons. By using SEAs, nonlinearities inherent in the transmission system were eliminated, resulting in accurate torque control [9], [22]. Additionally, SEAs enable the implementation of a force control without the requirement for a costly force sensor since the output torque can be directly calculated from its spring characteristics. However, SEAs have low bandwidth and low stiffness [23], also the SEAs are inefficient and use an excessive amount of power to operate. Moreover, SEAs with a high degree of freedom are complex and costly, which can complicate the project's implementation.

To address the issues associated with SEAs, a cable-driven mechanism has been developed [3], [20], [21]. This device transmits torque to adjacent components via cables. Torque amplifying for this approach is simply achieved by the use of a pulley system which can reduce the complexity and cost of the design and implementation. Mechanically, the cable-driven mechanism offers great compliance, low inertia, high stiffness, and is highly back-drivable all of which contribute to the robot safety and reliability. However, earlier implementation of this technique has remained bulky and difficult for users to wear and maneuver. Furthermore, the high transmission ratio cannot be achieved within a compact design.

In this paper, we presented a novel knee exoskeleton robot based on a cable-driven mechanism, with the objectives of enhancing human-machine interaction safety and device portability. The impedance controller based on an assist-as-needed approach was implemented in our design to ensure high users' safety and a possible better treatment outcome [3], [23]. Four experiments were carried out to assess the design's performance: the

mechanical transparency, active-assistive trajectory tracking, resistance of trajectory tracking, and gait cycle rehabilitation. The rest of this paper is structured as follows. Section II discusses the design criteria and detailed design of the mechanical components. Section III discusses the robot driving system and control architecture. Section IV describes the experimental setup and analyses the experiment's outcomes, while Section V provides a summary of the experiment's findings.

2. Mechanical Design

The proposed knee exoskeleton as depicted in Fig. 1 was developed for gait and knee rehabilitation. Unlike typical industrial robots, the design objectives for typical exoskeleton robots are focused on ensuring maximum safety for the users. So that in our design, the robot must have lightweight, low mass and low inertia, high back drivability, low friction, and highly compliant. Additionally, the attachment components and robot's frame must fit comfortably on any user, minimizing any unwanted strain during operation. The next section describes the design criteria and detailed design of the robot and the actuation system.

2.1. Design Criteria and Detailed Design of Mechanical Components

The following design specifications must be addressed to achieve a high level of safety performance: First, the robot's maximum weight should not exceed 2.5 kg, enabling the user to maneuver the leg effortlessly. Second, the robot's joints and attachments or frame must be designed anthropomorphically to allow the user to comfortably wear the exoskeleton. This may be achieved by considering that the robot's joint must be capable of rotating in one degree of freedom between 0 and 110 degrees in the sagittal plane, and both the shank and thigh braces must comfortably fit a person standing between 160 and 185 cm tall. In addition to the mechanical design, the robot should be capable of producing a torque of at least 8 Nm, which is about half of the torque required for normal walking of healthy persons in the knee joint. Finally, the transmission should have low friction, high back drivability with zero backlash, and exhibit great compliance.

To meet the design criteria, a novel design of power transmission based on cable-driven has been developed as shown in Fig. 2. The proposed cable-driven of the exoskeleton consists of four major components: a calf brace, a thigh brace, an output flange, and a power unit.

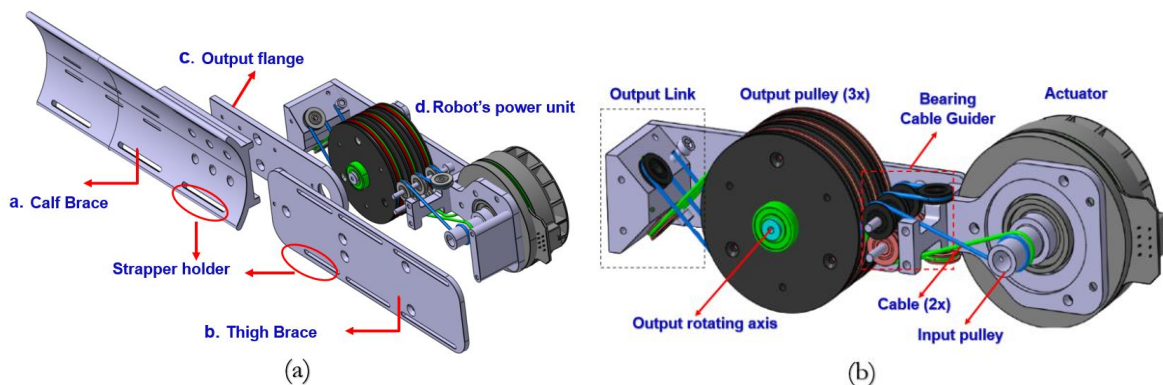


Fig. 2. Mechanical design and components used in the proposed robot. (a) overall components. (b) the novel cable-driven transmission mechanism.

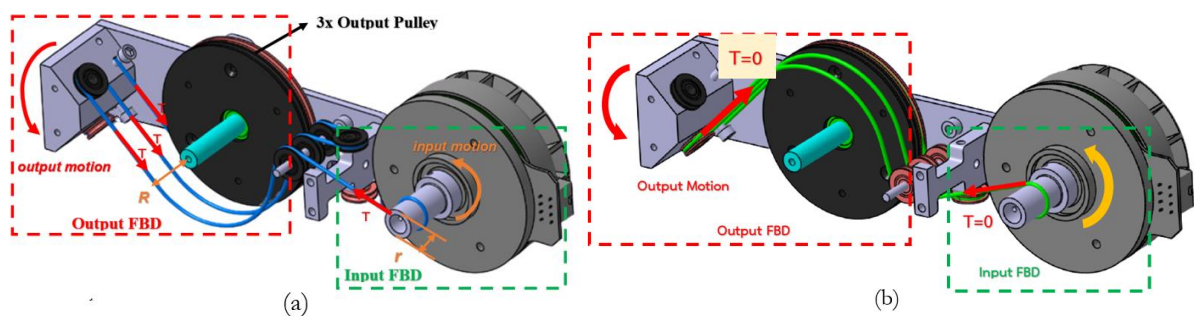


Fig. 3. Free-body diagram (FBD) of the mechanism under counterclockwise rotation of the motor. (a) FBD of the mechanism for blue cable. At input side, the motor rotates in a counterclockwise direction generating torque with tension (T) and radius r . At the Output FBD, the output link is pulled down-counterclockwise by three cables ($3T$) with the radius of R around the rotating axis. (b) FBD of the green cable attached to the pulley of the mechanism. The green cable does not create any tension force due to slack in the cable as the motor rotates.

The total weight of the robot is 2.1 kg. And to assure comfort for the user, the ABS calf brace was designed to suit the users leg comfortably. The thigh brace, on the other hand, was made from aluminum to reduce the robot's weight while maintaining a high strength to withstand the substantial internal load. The soft strap is allowed the users to adjust the tightening force to minimize strain during operation. Additionally, to reduce weight, the output flange and the majority of the components of the robot's frame are made of aluminum. The primary function of this component is to transfer power from the actuator to users with a small amount of inertia

2.2. Actuation System and Power Transmission

The detailed design of the novel cable-driven mechanism is shown in Fig. 2 and Fig. 3. The Maxon EC90 brushless dc motor, capable of providing continuous torque of 533 mNm, is used as the actuator. The motor torque is then transmitted to an input pulley that has two cables wrapped around in opposite directions of each other: the green cable for clockwise movement and the blue cable for counterclockwise movement. This cable-driven mechanism transfers and amplifies torque using two distinct techniques: a block and tackle system, and a pulley-system mechanism. For the block and tackle system, the tension is amplified by the number of total cables attached to the output pulley ($N=3$). And, in the case of a pulley-system mechanism, the torque is amplified by the difference in diameter between the input and output pulley. By arranging the cables as illustrated in Fig. 2, the free-body-diagram (FBD) can be shown in Fig. 3, and the gear ratio can be derived as follows:

$$\begin{aligned} \tau_{output} &= 3T_{cable} \times R \\ T_{cable} &= \frac{\tau_{input}}{r} \\ \tau_{output} &= 3 \frac{R}{r} \tau_{input} \end{aligned} \tag{1}$$

where r and R are the radius of the input and output pulley, respectively. When substituting $R = 40$ mm, and $r = 7.5$ mm, the total output torque is obtained as follows:

$$\tau_{output} = 3 \frac{40}{7.5} \tau_{input} = 16\tau_{input} \tag{2}$$

From Eq. (2), the novel cable-driven can amplify the torque 16 times when both the block and tackle system and pulley-system mechanism are used together. This mechanism, however, imposes constraints on the design. The next section will discuss the symmetry constraints. If the cables aren't wrapped in the other way, the mechanism becomes redundant and cannot move due to zero net torque. And, both cables must move symmetrically to prevent slack throughout the process.

2.3. Symmetry Constraint of the Mechanism

As shown in Fig. 4, the mechanism requires two cables, a blue cable, and a green cable, wrapped around in the opposite direction in order to rotate in both directions. Because the cable is capable of generating only tension, each cable in the mechanism can only provide either extension or flexion movement. Figure 4 depicted the FBD of the mechanism under a flexion movement

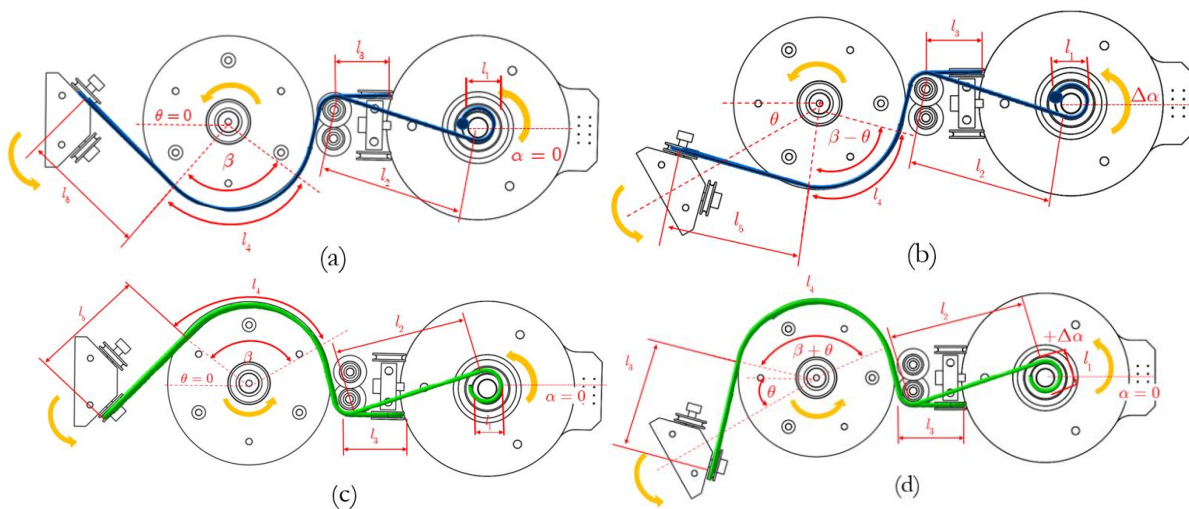


Fig. 4. Cables length of the mechanism at different stages when motor rotate in the counterclockwise direction. (a) blue cable at the initial stage. (b) blue cable at the arbitrary stage. (c) green cable at the initial stage. (d) green cable at the arbitrary stage.

The motor is required to move in the counterclockwise direction and the tension is generated only in the blue cable to pull down the output link. The green cable, on the other hand, is loosened by its wrapping direction and did not provide any tension. This allowed the output link to rotate freely without the interference of inverted torque from the green cable. Equation (3) demonstrates the net torque calculation of the mechanism under flexion movement:

$$\begin{aligned} \sum \tau &= I\ddot{\theta} \\ \tau_{blue} - \tau_{green} &= I\ddot{\theta} \\ \tau_{blue} &= 3T_{blue} \cdot R = I\ddot{\theta} \end{aligned} \quad (3)$$

From Eq. (3), only the blue cable generates the tension to rotate the mechanism. If the green cable is wrapped around the motor in the same direction as the blue cable, the net torque on the output link will be zero, and the mechanism remains stationary in either direction.

Additionally, the two cables must move in a symmetrical relationship throughout the operation to ensure that neither cable becomes loosened. When one cable goes in one direction, the opposing cable must travel an equal length in the opposite direction. The relationship between the length of each cable can be derived from Fig. 4, where it is assumed that both cables are initially under full tension. Six variables are shown in the illustration: r is the radius of the input pulley, R is the radius of the output pulley, α is the motor's angle, β is the cable angle at the output pulley, θ is the angle of output pulley, and l is the cable's length for each location. Therefore, the total length for each cable is:

$$l_{tot} = l_1 + l_2 + l_3 + l_4 + l_5$$

where the l_2, l_3, l_5 are constant. If the motor rotates counterclockwise from an initial position ($\alpha=0$ and $\theta=0$) to any arbitrary position ($\alpha=\alpha_2$ and $\theta=\theta_2$), the change in cable length can be derived as follows:

$$\begin{aligned} \Delta l_{tot} &= \Delta l_1 + \Delta l_4 \\ \Delta l_{tot} &= \frac{\pi}{180} r \Delta\alpha + n \frac{\pi}{180} R \Delta\theta \\ \Delta l_{tot} &= \frac{\pi}{180} r \Delta\alpha + n R \Delta\theta \end{aligned} \quad (4)$$

where n represent the number of the output pulley. Then, the change in length for each cable is:

$$\begin{aligned} \Delta l_{tot,blue} &= \frac{\pi}{180} r \alpha_2 - n R \theta_2 \\ \Delta l_{tot,green} &= \frac{\pi}{180} - r \alpha_2 + n R \theta_2 \\ \Delta l_{tot,blue} &= -\Delta l_{tot,green} \end{aligned} \quad (5)$$

From Eq. (5) and Fig. 4, it can be concluded that the relationship between the change in two cables' lengths is completely symmetrical and in the opposite direction of each other. That is, when the motor rotates counterclockwise, the motor's angle

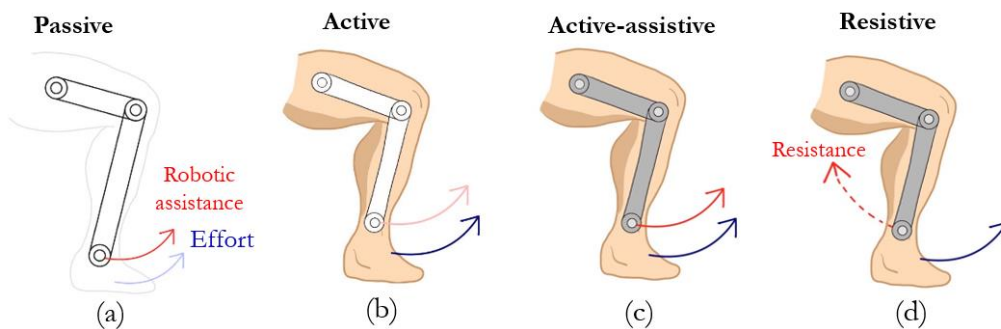


Fig. 5. Four types of training modalities. (a) Passive modality. The robot completes the task without the user exerting any effort. (b) Active modality. The users make effort to perform the task independently, without the intervention from the robot. (c) active-assistive modality. Both user and robot collaborate to complete the task. The robot will provide just enough assistive force so that the user can perform or complete the task on his own. (d) Resistive modality. The robot counteracts a user's effort by providing resistance force.

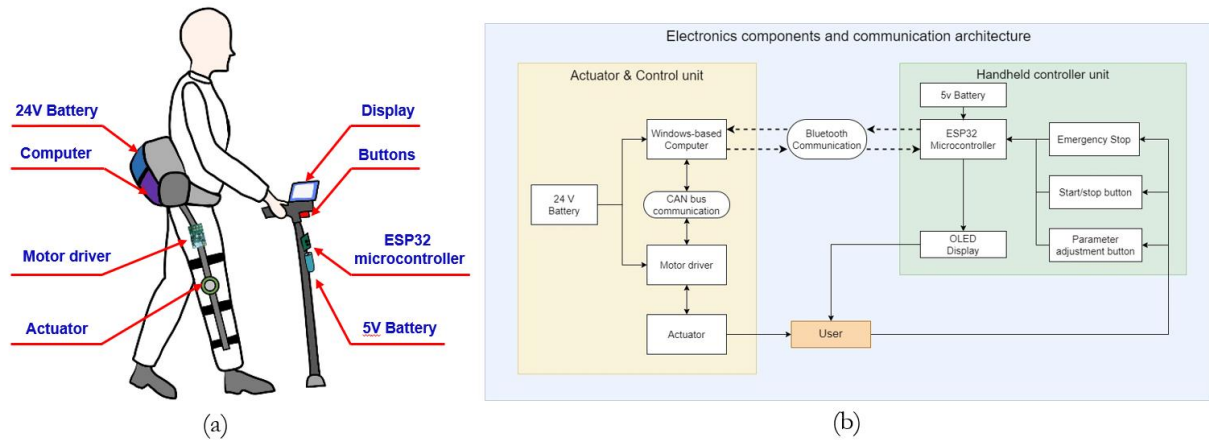


Fig. 6. Electronic components and communication architecture of the proposed robot system. (a) Electronic components of two subunits: Actuator & Control unit and Handheld controller unit. (b) Communication flow and use diagram of the robot system.

for the blue cable α_{blue} increases while the output's angle θ_{blue} drops; conversely, the motor's angle for the green cable α_{green} declines while the output's angle θ_{green} increases. And Eq. (5) is true regardless of the motor's rotating direction. Furthermore, we can substitute the gear ratio from Eq. (2) into Eq. (5) to investigate the cable tension.

$$\begin{aligned} \Delta\alpha &= \Delta\theta \cdot GearRatio \\ \Delta\alpha &= \Delta\theta \left(\frac{nR}{r} \right) \\ \Delta l_{tot,blue} &= \frac{\pi}{180} \left(r\Delta\alpha - nR \left(\frac{r\Delta\alpha}{nR} \right) \right) = 0 \end{aligned} \quad (6)$$

From Eq. (6), the difference in length between any two arbitrary locations is always zero, indicating that both cables are always in tension. As a result, this mechanism can rotate in both clockwise and counterclockwise directions without cable get loosen. Additionally, based on Eq. (5) and Eq. (6), the use of single motor to control the tension on two cables is achievable without introducing redundancy in the system.

3. Electronics and Control Architecture

This section discusses the robot driving system and control architecture used in the mechanism. In this research, two distinct forms of training modalities are implemented: active-assistive modality and resistive modality. As shown in Fig. 5, the training modalities are classified according to the physical interaction between the user and the robot

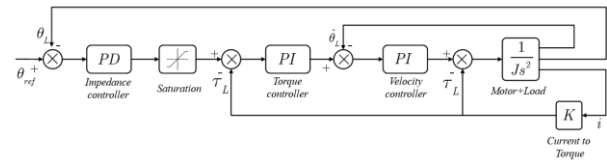


Fig. 7. Block diagram of the impedance controller based on active-assistive modality.

during the operation. In the case of active-assistive modality, the robot provides an assistive force to support the user's motion. However, in resistive modality, the robot delivers resistance force to counteract the user effort. The two training modalities apply impedance controller as a low-level control technique that can measure the user effort and use it to control the human-machine interaction.

3.1. Electronics components and communication architecture.

The electronics and communication architecture of the proposed robot are comprised of two wirelessly linked subunits: an actuator and control unit and a handheld controller unit, as shown in Fig. 6. The Actuator & Control unit consists of four components: a computer, a 24V battery, a motor driver, and an actuator that is worn on the wrist and thigh of the user. This unit's primary function is to create torque to aid in the rehabilitation of patients. To begin, the windows-based PC serves as the primary controller, calculating and producing control signals in real time to regulate the robot's output force and velocity. The control signals are then communicated to the Copley control Accelnet motor driver through CAN bus connection, which requires low hardware space and contributes to the robot's lightweight design. Following that, the actuator receives the signal and creates torque in response to the control signals. The force, for the torque control strategy, can be estimated through the measure of a current required by the motor. The actual measurement of force using a force/torque sensor is not required in our

system. In this system, a 24V battery serves as the main power supply for both the PC and the actuator. Finally, an motor-integrated encoder is implemented as the position sensor in this design.

The Handheld controller unit, as seen in Fig. 6, consists of six components: an ESP32 microcontroller, an OLED display, a 5V battery, an emergency-stop switch, a start/stop button, and a parameter adjustment button. The major objective of this unit is to enable users to control the robot remotely. This unit is mounted to the top of a walking cane and has an OLED display, which enables users to manage the robot simply by pressing the button and monitor its status while holding it in their hand. The parameter adjustment button allows users to choose between cycling, walking, and teaching modes, as well as between active-assistive and resistive controls. Additionally, users can adjust the speed and maximum assistance of the robot to personalize the treatment. Then, by signaling the start/stop button, users may initiate or stop the motion. And finally, the ESP32 microcontroller detects all button signals and transmits them to the PC via Bluetooth connection.

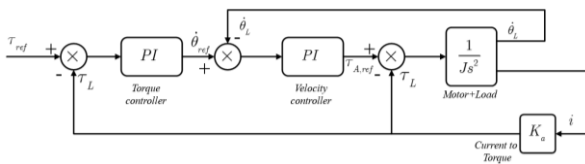


Fig. 8. Block diagram of the impedance controller based on resistance approach.

3.2. Active-Assistive Modality

As the primary goal of rehabilitation robot development is to maximize treatment outcomes, this may be accomplished by increasing user engagement and actively involving the user effort in the rehabilitation processes [24]. The active-assistive control technique allows users to put their effort toward task completion while the robot assists them partially and only to the extent that it is needed by the users. In another word, the robot will provide just enough assistive force so that the users can perform or complete the task on their own.

As shown in Fig. 7, the active-assistive control technique consisted of 3 cascade loops. Starting with the outer loop, the motion control loop, an impedance controller using characteristic of the Proportional-Derivative (PD) algorithm to generate a reference torque signal for the next loop. The control law for a reference torque is shown in Eq. (7).

$$\tau_{ref} = K_p (\theta_{ref} - \theta_L) + K_d (\dot{\theta}_{ref} - \dot{\theta}_L) \quad (7)$$

The proportional controller gain k_p is selected substantially higher than derivative gain k_d so that the generated torque reference signal will behave like a spring

with smooth movement or reduce the rapid change of velocity. The torque reference will be limited to the maximum assistive torque which can be adjusted personally for each user.



Fig. 9. Experimental setup for the active-assistive and resistive experiment.

For the middle loop, the Proportional-Integral (PI) controller is used to generate torque control signal in the system. The actual torque of the system can be estimated from the current sensor embedded in the motor driver. Thus, the difference between the reference torque command and actual torque can be calculated and used in the PI-control law to generate the velocity command. Lastly, the inner velocity loop. The actual velocity can be estimated by differentiating the measured motor angular position with a low-pass filter. Then, the velocity error can be calculated and utilized in conjunction with PI-control law to provide a control signal for robot motion control.

This control strategy also enables an assist-as-needed (AAN) technique. The robot assists patients with just enough assistive force, allowing patients to control their movements with his exerting effort. This means, that if the patient can perform the given task on his own, the robot will not provide any assistive force. However, if the patients are unable to perform the given task, the robot will provide just enough assistive force to help the user to complete the task. The maximum assistive force is adjustable for safety purposes. Thus, this control architecture is better suited to patients who are severely impaired or who are in the early stages of stroke rehabilitation.

3.3. Resistive Modality

In contrast to the active-assistive approach, the resistive modality actively resists the users movement in order to strengthen their muscles. As a result, this approach is recommended for patients with mild impairment, and not for those in the early stages of stroke rehabilitation. It is also good for people who want to build up their muscles such as sports rehabilitation after surgery. The resistive controller architecture, as shown in Fig. 8, composes of two cascade loops: torque control and velocity control loop. The reference torque for the torque control loop in this system is derived using Eq (8).

$$\tau_{ref} = -K_{damp} \cdot \dot{\theta}_{ref} - \dot{\theta}_L \quad (8)$$

The reference torque is proportional to the joint angular velocity in the inverse direction. In other words, the reference torque serves as a damper to resist the knee joint motion of the users. The faster the users attempt to move the leg, the greater the resistance force created by the robot. A PI-controller is used in this torque control loop to improve the system's torque tracking performance. Following with the velocity control loop, the PI-controller is implemented in this loop to ensure the velocity control as well as the reference torque, τ_{ref} . This will make the system more robust as in the active-assistive controller.

4. Experiment Result and Discussion

In this study, we propose four extensive experiments to evaluate the performance of the suggested exoskeleton system. The experimental procedures are detailed in this part, followed by the findings and their interpretation. To begin, an analysis of mechanical transparency was performed to determine the robot's back drivability and mechanical performance. Second, an active-assistive trajectory tracking experiment was conducted to evaluate the active-assistive controller performance during human operation. Thirdly, a resistance of trajectory tracking experiment was studied to evaluate the resistance controller's effect on the users. Finally, the gait rehabilitation experiment based on teach-and-repeat approach was performed to evaluate the effectiveness and initial feasibility of the robotic gait rehabilitation. The first experiment was conducted entirely on the robot without a human subject involved. However, the second, the third, and the final experiments were performed on two participants who did not have any documented on lower-limb physical injuries or gait impairment. The demographic characteristics of the two subjects, including their gender, age, height, and mass, are summarized in Table 1.

Table 1. Demographic information of the subjects participated in the experiments.

Parameters	Subject 1	Subject 2
Gender	Male	Female
Age (years old)	25	26
Height (cm)	175	170
Mass (kg)	65	59
Status	Healthy	Healthy

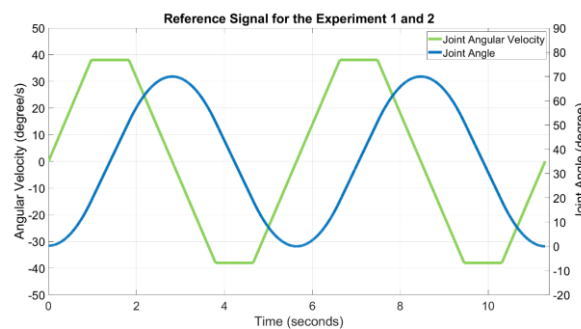


Fig. 10. Trapezoidal velocity profile and corresponding position signal. The maximum joint angular velocity and position is 39.0 degree/s and 70 degrees respectively. Each cycle takes 5.80 seconds to complete.

4.1. Mechanical Transparency

A mechanical transparency analysis was done to determine the exoskeleton robot's back drivability. To determine the mechanism's transparency, the motor was required to track the position reference signal with no external load attached to the robot. Then, the output torque of the robot's joint is measured and analyzed to get the root mean square average (RMS) of torque, as denoted by $\bar{\tau}$. As shown in Fig. 11, the required operation torque range for the mechanism to operate is within ± 1.02 Nm range and has a RMS value of 0.457 Nm. By comparing this no-load torque to our 16-times transmission ratio, it is shown that the proposed design is highly transparent and backdrivable. According to a previous research [8], the measured RMS torque under no-load conditions is 1.03 Nm. When compared to our finding of 0.457 Nm, our proposed robot could considerably lower passive mode torque by more than 50%, implying that the proposed exoskeleton can offer a high level of safety during human-machine interaction.

4.2. Active-assistive Trajectory Tracking Experiment

To evaluate the performance and feasibility of the active-assistive modality, an intensive position tracking, based on an impedance controller, was undertaken. During a sitting posture, the robot's joint was attached to the subject's knee and the knee motion will be controlled by the mechanism to track a trapezoidal velocity profile as shown in Fig. 10. The maximum velocity and acceleration of the referenced trapezoidal velocity profile can be adjusted. Before the experiment, the base-torque, the torque required to hold the knee at a constant 70-degree angle, was obtained by measuring the torque of the mechanism required to lift the knee extension without any lifting effort from the subject. The required base-torque was 3.3 Nm for subject 1 and 3.0 Nm for subject 2. This base-torque was used to set a limit on the maximum robotic-assistance torque provided by the impedance controller, which was selected as the experimental variable. As stated in Table 2, the maximum robotic-assistive force was set at

50%, 75%, 100%, 125%, and 150% relative to the base-torque for each subject.

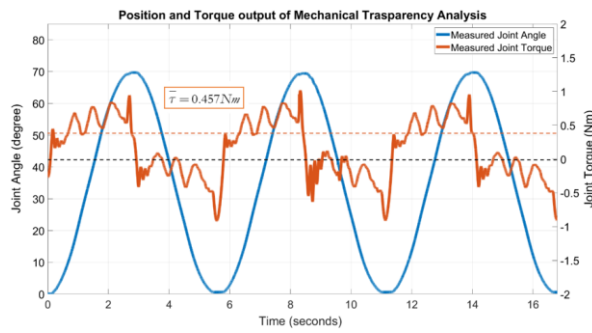


Fig. 11. The result of position tracking under no-load conditions for mechanical transparency analysis. The highest torque value is 1.02 Nm, and the RMS torque is 0.457 Nm. The positive torque indicates the knee extension while the negative value expresses the knee flexion.

For each experimental case, the knee with attached mechanism was controlled to follow the reference motion for seven cycles in a sitting posture. For the first two and the last two cycles, the subjects were instructed not to exert any effort. The knee motion was controlled by the mechanism only. During the three center cycles, however, the subjects were required to apply their effort to follow the position reference. As shown in Fig. 12, Fig. 13, and Table 2, the plot can be divided into 2 zones: The No-Effort zone and the Effort zone. Two metrics were calculated for each zone to evaluate the performance characteristics as described in Eq. (9): the root-mean-square (RMS) of position error ($\bar{\theta}_{e,NE}$, $\bar{\theta}_{e,E}$) and the RMS of robotic-assistive torque ($\bar{\tau}_{NE}$, $\bar{\tau}_E$). The NE and E subscripts are referred to as the No-Effort and Effort zones. Additionally, the grand mean ($\bar{\bar{\theta}}$ and $\bar{\bar{\tau}}$) and grand standard deviation are calculated as statistics for each zone according to Eq. (10). The grand mean was calculated by taking a simple numerical average of all five cases for each metric and the grand standard deviation was calculated by computing the variance from the grand mean by assuming the normal distribution approach.

$$\left\{ \begin{aligned} \theta_{error,rms} = \bar{\theta}_e &= \sqrt{\frac{\sum_{i=1}^N \theta_{ref} - \theta_i^2}{N}} \\ \tau_{rms} = \bar{\tau} &= \sqrt{\frac{\sum_{i=1}^N \tau_i^2}{N}} \end{aligned} \right. \quad (9)$$

$$\left\{ \begin{aligned} \bar{\bar{\theta}}_e &= \frac{1}{N_{case}} \sum_{i=1}^{N_{case}} \bar{\theta}_e \\ \bar{\bar{\tau}} &= \frac{1}{N_{case}} \sum_{i=1}^{N_{case}} \bar{\tau}_e \end{aligned} \right. \quad (10)$$

Three significant findings are highlighted in the study. First, the position error and robotic-assistance torque in the Effort zone ($\bar{\theta}_{e,E}$ and $\bar{\tau}_E$) are significantly lower than those in the No-Effort zone ($\bar{\theta}_{e,NE}$ and $\bar{\tau}_{NE}$) as seen from the grand mean for both subjects. The RMS of position error ($\bar{\theta}_e$) decreases by 79.7% and 28.0% for subject 1 and 2 and RMS of robotic-assistive torque ($\bar{\tau}$) also decreases by 70.8% for subject 1 and 79.9% for subject 2 when changing from the No-Effort zone to the Effort zone. Second, for the No-Effort zone, increasing the allowable maximum robotic-assistive torque resulted in a decrease in position error $\bar{\theta}_{e,NE}$ and an increase in robotic-assistance torque $\bar{\tau}_{NE}$.

Finally, in the Effort zone, increasing the maximum allowance of robotic-assistive torque has little effect on measured torque or position error.

As shown in Table 2, and Table 3, the grand standard deviation of position error in the Effort zone are 2.88 degrees and 1.44 degrees and the robotic-assistive torques are 0.08 Nm and 0.22 Nm for the subject 1 and subject 2, respectively. The low standard deviation and mean of statistics during the Effort zone indicated that the subject was capable of exerting sufficient effort to complete the task on their own and that the robot did not interfere with the subject during the operation.

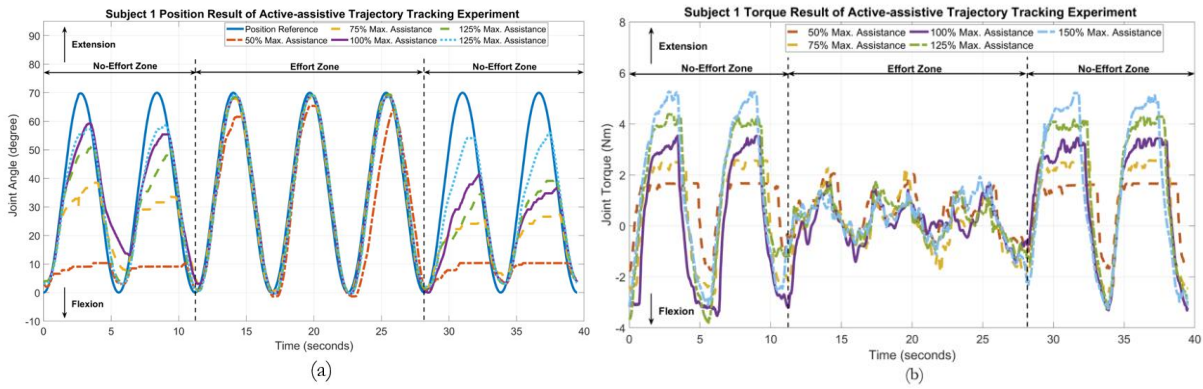


Fig. 12. Results of the active-assistive trajectory tracking experiment of subject 1 varied by the maximum robotic-assistance torque. The based-torque (100% Max. Assistance) for subject 1 is 3.3 Nm. The vertical dashed lines denote the boundary between No-Effort and Effort zones. The positive torque and position indicate the knee extension whereas the negative values demonstrate the knee flexion. A total of seven-position cycles are generated with the first couple and the last couple cycles are in the No-Effort zone while the middle three cycles are in the Effort zone. (a) the joint angle of subject 1 in the experiment. The blue solid line denotes the position reference trajectory. Whereas other dashed curves indicate the actual joint angle for each case. (b) Joint torque of subject 1 corresponding to the position reference.

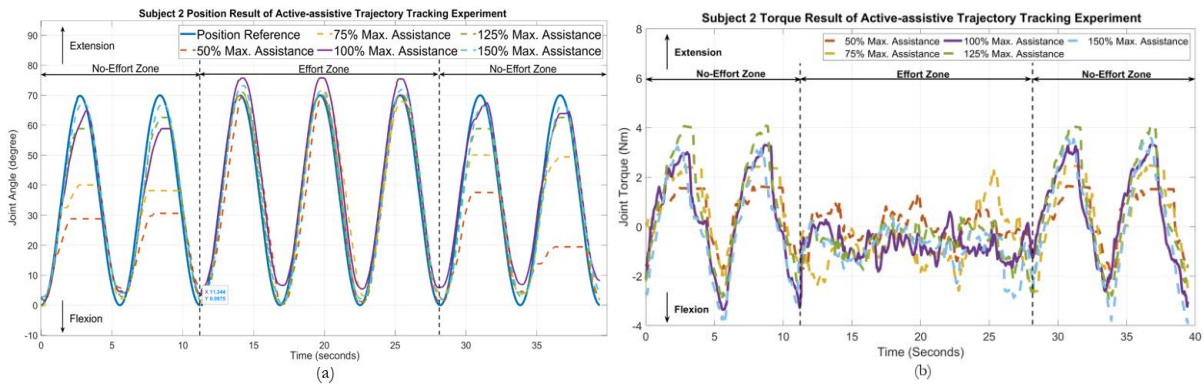


Fig. 13. Results of the active-assistive trajectory tracking experiment of subject 2. The based-torque (100% Max. Assistance) for subject 2 is 3.0 Nm. (a) the joint angle of subject 2 in the experiment. (b) the joint torque of subject 2 corresponding to the position reference.

Table 2. Result of Active-assistive trajectory tracking experiment of subject 1.

Case	Max. Assistance (Nm)	$\bar{\theta}_{e,NE}$ (deg.)	$\bar{\theta}_{e,E}$ (deg.)	$\bar{\tau}_{NE}$ (Nm)	$\bar{\tau}_E$ (Nm)
50%	1.65	35.5	9.59	1.48	0.95
75%	2.48	22.5	1.81	2.13	0.96
100%	3.30	16.44	3.98	2.64	0.83
125%	4.13	17.9	4.11	3.07	0.77
150%	4.95	9.80	4.30	3.32	0.83
Grand Mean		20.44	4.76	2.53	0.87
Grand Standard Deviation		9.58	2.88	0.74	0.08

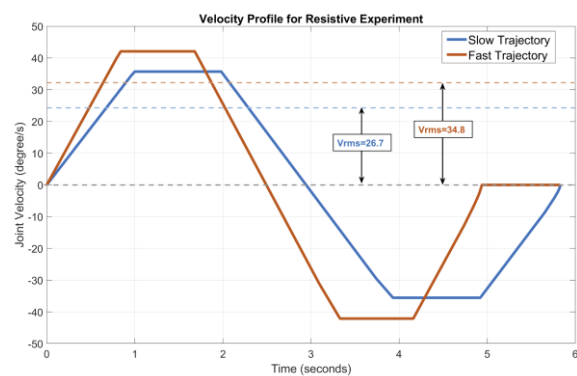


Fig. 14. The fast trajectory (red) and the slow trajectory (blue). The slow trajectory has an RMS velocity of 26.7 deg/s, while the fast trajectory has an RMS velocity of 34.8 deg/s.

4.3. Resistance of Trajectory Tracking Experiment

To determine the effectiveness and feasibility of the resistive modality technique, a resistance of trajectory tracking experiment is conducted using the resistance controller, as shown in Fig. 8. Two subjects were instructed to follow the reference velocity signals, which are a trapezoidal shape and comprise two modes: slow trajectory and fast trajectory, as illustrated in Fig. 14. Subjects were required to complete a total of eight cycle tracking task while seated: four cycles for slow trajectory and four cycles for fast trajectory. In this experiment, the exoskeleton system did not provide any assistance to help the subjects complete the tasks, instead, the exoskeleton resisted the subjects' movement as followed in Eq. (8). Three damping constants as shown in Eq. (11), considered low damping, medium damping, and high damping, were used in the experiments.

$$\begin{cases} k_{damping,low} &= 36 \text{ mNm/deg/s} \\ k_{damping,medium} &= 48 \text{ mNm/deg/s} \\ k_{damping,high} &= 60 \text{ mNm/deg/s} \end{cases} \quad (11)$$

Two significant results can be drawn from this experiment. Firstly, both participants demonstrated higher joint torque for the fast trajectory under the same damping constant, as shown in Fig. 15 and Fig. 16. Joint torque was increased by an average of 28.5 percent by only adjusting the reference velocity profile. Additionally, resistive torque indicated a significant correlation with the damping constants. The resistive torque was proportional to the damping constant; the higher the damping constant, the larger the resistive torque provided by the exoskeleton. The highest Root Mean Square (RMS) of resistive torque occurred during the high damping constant and fast trajectory condition with the value of 2.25 Nm for the subject 1 and 2.00 Nm for the subject 2. In contrast, the condition of slow trajectory and low damping constant resulted in the lowest resistive torque of 1.02 Nm for the subject 1 and 0.94 Nm for the subject 2.

Table 3. Result of Active-assistive trajectory tracking experiment of subject 2.

Case	Max. Assistance (Nm)	$\bar{\theta}_{e,NE}$ (deg.)	$\bar{\theta}_{e,E}$ (deg.)	$\bar{\tau}_{NE}$ (Nm)	$\bar{\tau}_E$ (Nm)
50%	1.50	22.79	6.43	1.25	0.61
75%	2.25	13.12	5.94	1.75	1.25
100%	3.00	5.98	6.44	2.01	0.91
125%	3.75	5.21	2.66	2.35	0.86
150%	4.50	4.65	4.59	2.11	1.11
Grand Mean		7.24	5.21	1.89	0.95
Grand Standard Deviation		3.43	1.44	0.38	0.22

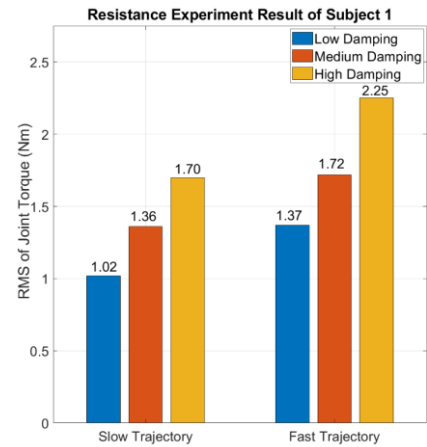


Fig. 15. Result of Resistance of trajectory tracking experiment of subject 1. The height of bar graph denotes the RMS value of measured joint torque. The highest resistance torque occurs at the fast trajectory and high damping condition with the value of 2.25 Nm.

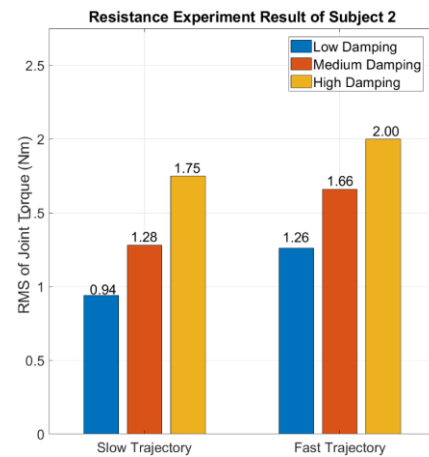


Fig. 16. Result of Resistance of trajectory tracking experiment of subject 2. Similarly, the fast trajectory and high damping condition contribute to the highest resistance torque of 2.00 Nm.



Fig. 17. Experimental setup and parameters employed in the computation for gait rehabilitation. The stride length and cycle period are determined using the length and time frame from the initial to the completion of gait.

Table 4. Gait rehabilitation experiment result of subject 1.

Subject 1	Cycle Period (sec)	Stride Length (cm)	Peak angle (deg)	Peak Torque (Nm)
Teach	1.42	87	49.6	-
Step 1	1.89	68	45.5	2.73
Step 2	2.39	73	44.1	3.83
Step 3	2.26	80	44.8	2.52
Step 4	1.93	76	44.6	3.49
Average	2.12	74.25	44.8	3.14

Table 5. Gait rehabilitation experiment result of subject 2.

Subject 2	Cycle Period (sec)	Stride Length (cm)	Peak angle (deg)	Peak Torque (Nm)
Teach	3.03	74	78.5	-
Step 1	3.13	82	77.9	2.20
Step 2	3.23	72	79.2	2.57
Step 3	3.04	77	76.3	3.19
Step 4	3.10	76	77.4	2.37
Average	3.13	76.75	77.7	2.58

4.4. Gait Rehabilitation Experiment based on Teach-and-Repeat approach.

This experiment employed a teach-and-repeat strategy to determine the practicality of the proposed robot's primary aim of gait rehabilitation. The robot is designed for stroke rehabilitation. It is suitable for after-stroke patients who are not in severe conditions but can stand and balance initially on their own with additional assistance from the robot. Consequently, this experiment was undertaken on the two healthy participants stated in Table 1 to determine the rehabilitation feasibility. To begin, each participant needed to wear the mechanism at his knee and the gait trajectory for the individual participant was recorded. Each individual's joint angle and speed were recorded so that the robot could accurately repeat the same trajectory as he had been trained. The subjects were then asked to repeat the walking steps four times to evaluate their gait rehabilitation performance. At this development stage, the walking step can be repeated by pressing the hand switch in the participant's hand. In this experiment, the participants were instructed not to exert any effort during the gait cycle.

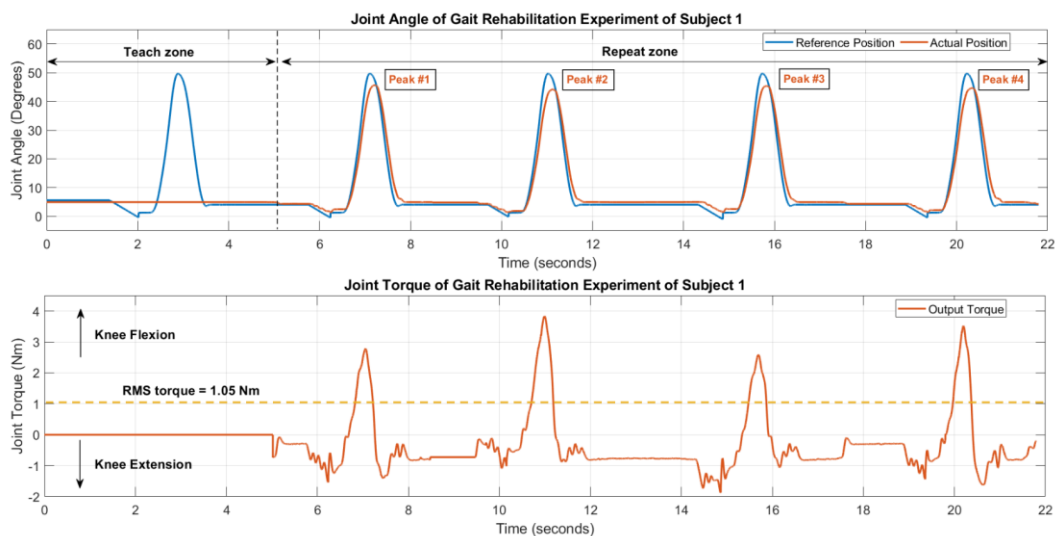


Fig. 18. The result of the Gait Rehabilitation Experiment of subject 1. The RMS torque is 1.05 Nm and occurred during the peak angle of the knee flexion.

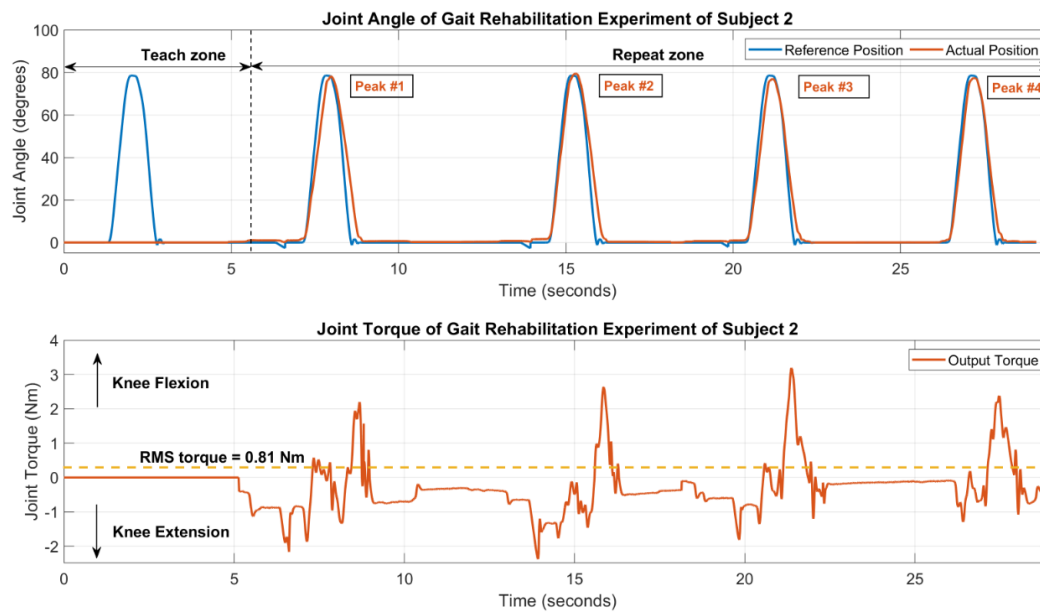


Fig. 19. The result of the Gait Rehabilitation Experiment of subject 2. The RMS torque is 0.81 Nm occurred during the peak angle of the knee flexion.

Figure 18 and Figure 19 display the experimental results for subject 1 and subject 2, respectively. The figure displays the relationship between reference trajectory, actual position, and associated torque of each walking step. The peak angle, peak torque, and RMS torque were measured to analyze the gait rehabilitation process. And finally, Table 4 and Table 5 conclude the experimental outcome for all matrices including cycle period, stride length, peak angle, and peak torque.

Subject 1's teach trajectory had a peak angle of 49.6 degrees, a cycle duration of 1.42 seconds, and a stride length of 87 cm. However, from the experiments, the actual value of the average peak angle was decreased to 44.8 degrees and the stride length was decreased to 74.25 cm. Throughout all stages, the average peak torque was 3.14 Nm with the RMS torque of 1.05 Nm. Additionally, subject 2 displayed a similar output pattern. The teach trajectory had a peak angle of 78.5 degrees, a stride length of 74 cm, and a cycle time of 3.03 seconds. Subject 2's actual stride length, peak angle, and cycle time, on the other hand, were all near to the taught value, with a stride length of 76.75 cm, peak angle of 77.7 degrees, and cycle period of 2.71 seconds. The average output torque was much less than that of subject 1, at 2.58 Nm and 0.81 Nm RMS value.

The results of the experiment indicated that the suggested robot could aid the subject in moving their leg with adequate torque to complete the gait cycle without the subjects exerting any effort. Even though the robot cannot perfectly track the recorded trajectory with zero position error and an identical cycle period, the participants can walk more than 2.97 m for subject 1 and 3.07 m for subject 2 over the four gait cycles, indicating that it is suitable to be used for gait rehabilitation applications that, normally, do not require high trajectory accuracy. Additionally, the experiments have been repeated for some time, and neither participant had any

negative effects during or after the experiment, confirming that the robot may be utilized safely for gait rehabilitation. These experiments have been done under the engineering aspect, a clinical trial for the after-stroke patients will be pursued by medical doctors.

5. Conclusion

In this paper, we proposed the design of a novel, lightweight, and highly back-drivable knee exoskeleton robot to raise the standard of safety in machine-human interaction. Mechanical transparency analysis is used to evaluate the safety and performance of a mechanical design. The results reveal that the proposed design is highly back drivable with little friction and no backlash introduced in the system. The active-assistive trajectory tracking experiment demonstrated that the proposed impedance controller was capable of ensuring very safe and reliable operation while also delivering an appropriate level of assistance corresponding with the assist-as-needed approach. For the resistance to trajectory tracking experiment, the exoskeleton displayed an appropriate range of resistive torque with adjustable damping constant to alter the interaction force between users and robot. And the last experiment, a teach-and-repeat gait rehabilitation experiment, demonstrated the high practicality of using robots in gait rehabilitation since the robot can deliver adequate torque to assist users in completing the gait cycle without additional effort. Moreover, two subjects who participated in the experiments showed no indication of negative effects during or after the robot operation. This means that the robot is safe and reliable to be used for stroke rehabilitation as well as exercise after knee surgery. And it can be used to assist a wide variety of patients with varying degrees of impairment, ranging from early stroke patients who require high assistance torque to those who require muscular strengthening through resistance training,

or it can be used in gait rehabilitation for patients with mild severity.

For future research, we intend to enhance the impedance control performance by improving the smoothness of the position and torque tracking response. We also plan to reduce the size and weight of the mechanism and improve the power transmission of the joint mechanism as well as safety and feasibility. The mechanism is ready for the clinical trial phase in varied aspects, and they will be done by medical doctors. The results of the clinical trial can be enhanced our mechanism to meet a medical device grade.

Acknowledgement

Part of this project is funded by National Research Council of Thailand (NRCT).

References

- [1] S. Li, G. E. Francisco, and P. Zhou, "Post-stroke hemiplegic gait: new perspective and insights," *Frontiers in Physiology*, p. 1021, 2018.
- [2] B. P. H. Chung, "Effectiveness of robotic-assisted gait training in stroke rehabilitation: A retrospective matched control study," *Hong Kong Physiotherapy Journal*, vol. 36, pp. 10-16, 2017.
- [3] A. Sutapun and V. Sangveraphunsiri, "A novel design and implementation of a 4-DOF upper limb exoskeleton for stroke rehabilitation with active assistive control strategy," *Engineering Journal*, vol. 21, no. 7, pp. 275-291, 2017.
- [4] P. Langhorne, F. Coupar, and A. Pollock, "Motor recovery after stroke: A systematic review," *The Lancet Neurology*, vol. 8, no. 8, pp. 741-754, 2009.
- [5] G. Kwakkel, B. Kollen, and J. Twisk, "Impact of time on improvement of outcome after stroke," *Stroke*, vol. 37, no. 9, pp. 2348-2353, 2006.
- [6] G. Chen, P. Qi, Z. Guo, and H. Yu, "Mechanical design and evaluation of a compact portable knee-ankle-foot robot for gait rehabilitation," *Mechanism and Machine Theory*, vol. 103, pp. 51-64, 2016.
- [7] H. Yu *et al.*, "Mechanical design of a portable knee-ankle-foot robot," in *2013 IEEE International Conference on Robotics and Automation*, 2013, pp. 2183-2188.
- [8] J. Wang *et al.*, "Comfort-centered design of a lightweight and backdrivable knee exoskeleton," *IEEE Robotics and Automation Letters*, vol. 3, no. 4, pp. 4265-4272, 2018.
- [9] K. Kong, J. Bae, and M. Tomizuka, "A compact rotary series elastic actuator for human assistive systems," *IEEE/ASME Transactions on Mechatronics*, vol. 17, no. 2, pp. 288-297, 2011.
- [10] S. Christensen *et al.*, "AXO-SUIT-A modular full-body exoskeleton for physical assistance," in *IFTOMM Symposium on Mechanism Design for Robotics*, 2018, pp. 443-450.
- [11] J.-H. Kim *et al.*, "Design of a knee exoskeleton using foot pressure and knee torque sensors," *International Journal of Advanced Robotic Systems*, vol. 12, no. 8, p. 112, 2015.
- [12] T. Eiammanussakul and V. Sangveraphunsiri, "Mechanical power to identify human performance for a lower limb rehabilitation robot," *Engineering Journal*, vol. 23, no. 4, pp. 91-105, 2019.
- [13] A. Plaza, M. Hernandez, G. Puyuelo, E. Garces, and E. Garcia, "Lower-limb medical and rehabilitation exoskeletons: A review of the current designs," *IEEE Reviews in Biomedical Engineering*, 2021. doi: 10.1109/RBME.2021.3078001
- [14] "ReWalk Robotics." <https://rewalk.com/>
- [15] J. L. Contreras-Vidal *et al.*, "Powered exoskeletons for bipedal locomotion after spinal cord injury," *Journal of Neural Engineering*, vol. 13, no. 3, p. 031001, 2016.
- [16] T. Eiammanussakul and V. Sangveraphunsiri, "A lower limb rehabilitation robot in sitting position with a review of training activities," *Journal of Healthcare Engineering*, vol. 2018, 2018.
- [17] G. Barbareschi, R. Richards, M. Thornton, T. Carlson, and C. Holloway, "Statically vs dynamically balanced gait: Analysis of a robotic exoskeleton compared with a human," in *2015 37th Annual International Conference of the IEEE Engineering in Medicine and Biology Society (EMBC)*, 2015, pp. 6728-6731.
- [18] R. W. Horst, "A bio-robotic leg orthosis for rehabilitation and mobility enhancement," in *2009 Annual International Conference of the IEEE Engineering in Medicine and Biology Society*, 2009, pp. 5030-5033.
- [19] "CYBERDYNE Inc." <https://www.cyberdyne.jp/english/>
- [20] Y.-J. Kim, "Design of low inertia manipulator with high stiffness and strength using tension amplifying mechanisms," in *2015 IEEE/RISJ International Conference on Intelligent Robots and Systems (IROS)*, 2015, pp. 5850-5856.
- [21] Y.-J. Kim, "Anthropomorphic low-inertia high-stiffness manipulator for high-speed safe interaction," *IEEE Transactions on Robotics*, vol. 33, no. 6, pp. 1358-1374, 2017.
- [22] N. C. Karavas, N. G. Tsagarakis, and D. G. Caldwell, "Design, modeling and control of a series elastic actuator for an assistive knee exoskeleton," in *2012 4th IEEE RAS & EMBS International Conference on Biomedical Robotics and Biomechanics (BioRob)*, 2012, pp. 1813-1819.
- [23] H. Vallery *et al.*, "Compliant actuation of rehabilitation robots," *IEEE Robotics & Automation Magazine*, vol. 15, no. 3, pp. 60-69, 2008.
- [24] S. Dalla Gasperina, L. Roveda, A. Pedrocchi, F. Braghin, and M. Gandolla, "Review on patient-cooperative control strategies for upper-limb rehabilitation exoskeletons," *Frontiers in Robotics and AI*, vol. 8, p. 745018, 2021.



Nattapat Kieuvongngam, photograph and biography not available at the time of publication.

Anan Sutapun, photograph and biography not available at the time of publication.

Viboon Sangeveraphunsiri, photograph and biography not available at the time of publication.